16th World Conference on Eeathquake Engineerign, 16WCEE 2017
Santiago Chile, January 9th to 13th 2017
Paper N3118
Registration Code: S-N1464177494

A MULTI-FIBER TIMOSHENKO BEAM FINITE ELEMENT WITH EMBEDDED DISCONTINUITIES FOR SEISMIC NONLINEAR CALCULATIONS

Ibrahim Bitar[*], **Nathan Benkemoun**[†], **Panagiotis Kotronis**[*] **and Stéphane Grange**[‡]

[*]École Centrale de Nantes, Université de Nantes, CNRS
Institut de Recherche en Génie Civil et Mcanique (GeM), UMR 6183
1 rue de la Noë, BP 92101, Nantes, cedex 3, France
e-mail: ibrahim.bitar@ec-nantes.fr ; panagiotis.kotronis@ec-nantes.fr

[†]IUT Saint-Nazaire, Université de Nantes, CNRS
Institut de Recherche en Génie Civil et Mcanique (GeM), UMR 6183
58 rue Michel Ange, 44600 Saint-Nazaire, France
e-mail: nathan.benkemoun@univ-nantes.fr

[‡]Université Grenoble Alpes, 3SR, F-38000 Grenoble, France
CNRS, 3SR, F38000 Grenoble, France
e-mail: stephane.grange@ujf-grenoble.fr

Key words: Timoshenko, Multi-fiber, Discontinuity

Abstract. A multi-fiber beam finite element based on the Timoshenko theory is proposed to simulate failure of reinforced concrete structural elements subjected to static or seismic loadings. The elements section can be of arbitrary shape and each fiber has a local constitutive law representing a specific material. The embedded discontinuity concept is adopted to enrich the fiber displacement field in order to describe crack openings and the development of plastic hinges. The material behavior at the discontinuity is characterized by a linear cohesive law linking the axial stress and the displacement jump, which permits to capture the released fracture energy. The variational formulation is presented in the context of the incompatible modes method followed by the corresponding computational procedure. Finally, two numerical applications are given to illustrate the performance of the proposed multi-fiber Timoshenko beam finite element.

1 Introduction

The development of robust and efficient numerical models to simulate the dynamic behavior of structures is mandatory in earthquake engineering. Nevertheless, the use of 2D or 3D finite element meshes requires high computational capacities due to the important number of the necessary degrees of freedom.

In order to simplify the global equilibrium equations and to reduce the required number of degrees of freedom different kinematic assumptions are often used in structural analysis. The Timoshenko beam theory considers that plane sections remain plane after deformation but not necessary normal to the deformed axis. The advantage of this theory is that it takes into account the influence of shear strains and has a very good performance in the context of dynamic calculations [1].

One of the first work introducing the idea of dividing a beam in "fibers", where a specific stress/strain relation is defined, is the book of Owen and Hilton [2]. Finite elements of this type are proven efficient for various applications in civil engineering: nonlinear analysis of beam type or bearing wall structures with non-homogenous sections [3], [4], arbitrarily geometrical plane or hollow shape sections [5], [6], bending, shear or torsion [7], Soil Structure Interaction [5], vulnerability assessment [6] and Fiber-Reinforced Polymer retrofitting problems [8].

We present hereafter a new multi-fiber Timoshenko beam finite element with embedded discontinuities to simulate failure of reinforced concrete structural elements subjected to static and dynamic loadings. The displacement-based formulation introduced in [9] is first adopted, with shape functions of order three (3) for the transverse displacements, two (2) for the rotations and an additional internal node resulting to a shear locking free finite element. The superior performance of this element with respect to other formulations found in the literature [11], [12] was already studied in [**?**]. In the following, an extension of the previous formulation is provided, introducing the embedded discontinuities concept.

If an internal length parameter is not considered in the adopted constitutive models, mesh dependency problems arise [13]. Under quasi-static loading conditions the equations governing the incremental equilibrium lose ellipticity, while under dynamic loading conditions wave speeds become imaginary [14]. Different approaches can be found in the literature to deal with this problem: local approaches [14], [15]; non local approaches [16], [17], [18]; enhanced approaches [19], [20]... In the following, we focus on the enhanced approach [20] and more specifically on the Embedded Discontinuity Approach (EDA) [21]. EDA represents an alternative way to the smeared and discrete crack representations avoiding some of their drawbacks as described in [22].

The EDA based on the strong discontinuity approach [20] is adopted hereafter, hence localized failure is incorporated into the standard displacement-based finite element formulation using additional variables. More specifically, the fibers are enhanced in order to describe concrete crack openings and the development of plastic hinges [23]. The strong discontinuity is introduced by adding a jump in the displacement field. Accordingly, additional shape functions are added to interpolate the displacement jump within the enhanced finite element. The material behavior at the discontinuity is considered using a linear decreasing cohesive law linking the axial stress and the displacement jump, which allows capturing the released fracture energy. The variational formulation is presented in the context of the incompatible modes method. Finally, the additional modes are statically condensed at the element level in order to decrease the necessary computational time.

The outline of the paper is as follows: in section 2, the governing equations of the multi-fiber Timoshenko beam (without and with embedded discontinuities) and the adopted interpolation functions [9] are briefly introduced. In section 3, we present the constitutive laws for the continuum and cohesive parts. In section 4, we focus on the variational formulation of the multi-fiber Timoshenko beam finite element with embedded discontinuities. Two numerical applications are presented in section 5. The article ends with some concluding remarks.

2 Governing equations

Consider a beam of length Ł discretized into n elements $e = [x_i; x_j]$ of length $L = x_j - x_i$ and external nodes i and j. The generalized displacement vector is approximated by an equation of the form $U(x) = NU_e$, where U_e is a vector containing the external nodal displacements of the element e and N is the matrix of the shape functions depending on x. For simplicity reasons the presentation hereafter is made in 2D.

$$U(x) = \begin{bmatrix} U_x(x) & U_y(x) & \Theta_z(x) \end{bmatrix}^T \tag{1}$$

$U_x(x)$ being the generalized longitudinal displacement, $U_y(x)$ the transverse displacement and $\Theta_z(x)$ the rotation of the section. The displacements $\overline{u}_x(x,y), \overline{u}_y(x,y)$ of another point of the section (or of a "fiber" $f(x,y)$) can be evaluated using the displacements of the section following the Timoshenko theory:

$$\begin{aligned} \overline{u}_x(x,y) =& U_x(x) - y\Theta_z(x), \\ \overline{u}_y(x,y) =& U_y(x) \end{aligned} \tag{2}$$

The strain field becomes:

$$\begin{aligned} \overline{\varepsilon}_x(x,y) =& \frac{\partial u_x}{\partial x} = U_x'(x) - y\Theta_z'(x), \\ \overline{\gamma}_{xy}(x,y) =& \frac{\partial u_x}{\partial y} + \frac{\partial u_y}{\partial x} = U_y'(x) - \Theta_z(x) \end{aligned} \tag{3}$$

with $\overline{\varepsilon}_x(x,y)$ the axial strain and $\overline{\gamma}_{xy}(x,y)$ the transverse shear strain of the fiber $f(x,y)$. The line over the variables indicates that they are continuous.

Using the equilibrium equations, the kinematic assumption and the virtual work principle, the stiffness matrix and the internal nodal forces of the multi-fiber Timoshenko element become:

$$\begin{aligned} K_{element} &= \int_0^L B^T K_S B dx \\ F_{int,element} &= \int_0^L B^T F_S dx \end{aligned} \tag{4}$$

where B is a matrix containing the derivatives of the shape functions with respect to x, K_S is the multi-fiber section stiffness matrix and F_S is the generalized force vector of the section.

In order to enhance the element kinematics, the fiber axial displacement field (2) is enhanced with an additional term [23], [24], [25], [26], as follows:

$$u_x(x,y) = \overline{u}_x(x,y) + \alpha M_\alpha(x), \tag{5}$$

where

- $M_\alpha(x) = H_\alpha(x) - N(x),$ (6)
- $H_\alpha(x) = \{1 \text{ if } x > x_\alpha \text{ or } 0 \text{ if } x \leq x_\alpha\},$ (7)
- $N(x) = \dfrac{x}{L},$ (8)

with α the discontinuity variable and x_α the position of the discontinuity within the element. The enhanced axial strain field becomes:

$$\begin{aligned} \varepsilon_x(x,y) =& \frac{\partial}{\partial x}\left(\overline{u}_x(x,y)\right) + \frac{\partial}{\partial x}\left(\alpha M_\alpha(x)\right) \\ =& \overline{\varepsilon}_x(x,y) + \alpha \frac{\partial}{\partial x}\left(-N(x)\right) + \alpha \frac{\partial}{\partial x}\left(H_\alpha(x)\right) \\ =& \underbrace{\overline{\varepsilon}_x(x,y) + \alpha \; G(x)}_{\tilde{\varepsilon}} + \underbrace{\alpha \, \delta_\alpha(x)}_{\overline{\overline{\varepsilon}}} \end{aligned} \tag{9}$$

where $\delta_\alpha(x)$ is the Dirac function at x_α. The expression of the axial strain is therefore singular (presence of $\overline{\overline{\varepsilon}}$). To deal with this singularity, [27] adopts a cohesive law, that models the material discontinuity and thus eliminates the singular term.

2.1 Displacement-based finite element formulation

In this section, the displacement-based finite element formulation introduced in [9] is briefly presented. The element is named Full Cubic Quadratic (FCQ), because Caillerie & al. [9] proved that one FCQ element is able to predict the exact tip displacements for any complex loading (shear/flexion) submitted to an homogeneous elastic beam (see also [**?**]). The element is free of shear locking and uses an additional internal node.

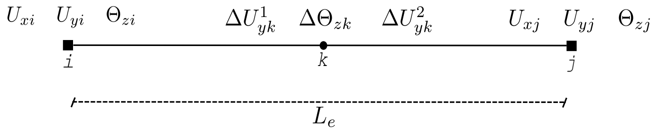

Figure 1: FCQ element

The nodal displacement field takes the following form

$$U_e^T = [U_{xi}, U_{yi}, \Theta_{zi}, \Delta U^1_{yk}, \Delta\Theta_{zk}, \Delta U^2_{yk}, U_{xj}, U_{yj}, \Theta_{zj}],$$

where ΔU^1_{yk}, $\Delta\Theta_{zk}$ and ΔU^2_{yk} are the degrees of freedom of the internal node (with no specific physical meaning). The interpolation functions of the FCQ element are [9]:

$$N(x) = \begin{bmatrix} N_1 & 0 & 0 & 0 & 0 & 0 & N_7 & 0 & 0 \\ 0 & N_{11} & 0 & N_{13} & 0 & N_{15} & 0 & N_{17} & 0 \\ 0 & 0 & N_{21} & 0 & N_{23} & 0 & 0 & 0 & N_{27} \end{bmatrix} \tag{10}$$

$$\text{where} \begin{cases} N_1 = 1 - \frac{x}{L_e} & N_{13} = 2(1-\frac{x}{L_e})^2(\frac{x}{L_e}) & N_{21} = (1-\frac{x}{L_e})(1-3\frac{x}{L_e}) \\ N_7 = \frac{x}{L_e} & N_{15} = -2(\frac{x}{L_e})^2(1-\frac{x}{L_e}) & N_{23} = 1-(1-2\frac{x}{L_e})^2 \\ N_{11} = (1-\frac{x}{L_e})^2(1+2\frac{x}{L_e}) & N_{17} = (\frac{x}{L_e})^2(3-2\frac{x}{L_e}) & N_{27} = -(\frac{x}{L_e})(2-3\frac{x}{L_e}) \end{cases} \tag{11}$$

The three internal degrees of freedom can be treated locally (in the element subroutine) using the static condensation method (see [9] for more details and the analytic expressions of the condensed matrices and vectors). We present hereafter the FCQ element mass matrix that becomes:

$$M_{element} = \begin{bmatrix} \frac{L_e S \rho}{3} & 0 & 0 & 0 & 0 & 0 & \frac{L_e S \rho}{6} & 0 & 0 \\ 0 & \frac{13 L_e S \rho}{35} & 0 & \frac{11 L_e S \rho}{105} & 0 & -\frac{13 L_e S \rho}{210} & 0 & \frac{9 L_e S \rho}{70} & 0 \\ 0 & 0 & \frac{2 I L_e \rho}{15} & 0 & -\frac{I L_e \rho}{15} & 0 & 0 & 0 & -\frac{I L_e \rho}{30} \\ 0 & \frac{11 L_e S \rho}{105} & 0 & \frac{4 L_e S \rho}{105} & 0 & -\frac{L_e S \rho}{35} & 0 & \frac{13 L_e S \rho}{210} & 0 \\ 0 & 0 & -\frac{I L_e \rho}{15} & 0 & \frac{8 I L_e \rho}{15} & 0 & 0 & 0 & -\frac{I L_e \rho}{15} \\ 0 & -\frac{13 L_e S \rho}{210} & 0 & -\frac{L_e S \rho}{35} & 0 & \frac{4 L_e S \rho}{105} & 0 & -\frac{11 L_e S \rho}{105} & 0 \\ \frac{L_e S \rho}{6} & 0 & 0 & 0 & 0 & 0 & \frac{L_e S \rho}{3} & 0 & 0 \\ 0 & \frac{9 L_e S \rho}{70} & 0 & \frac{13 L_e S \rho}{210} & 0 & -\frac{11 L_e S \rho}{105} & 0 & \frac{13 L_e S \rho}{35} & 0 \\ 0 & 0 & -\frac{I L_e \rho}{30} & 0 & -\frac{I L_e \rho}{15} & 0 & 0 & 0 & \frac{2 I L_e \rho}{15} \end{bmatrix} \tag{12}$$

where ρ represents the material density.

3 Constitutive laws

In the following, the constitutive laws for the continuum and cohesive materials are briefly elaborated (see figure (2)).

3.1 Concrete

In order to simulate concrete, a simple damage law based on the work of Ortiz 1985 [28] is adopted. The thermodynamic free energy for such model is expressed as function of the damage deformation $\overline{\varepsilon}^d$, the damage compliance modulus D and the strain-like hardening variable $\overline{\xi}^d$:

$$\overline{\Psi}^d = \overline{\sigma}^{dT}\overline{\varepsilon}^d - \frac{1}{2}\overline{\sigma}^{dT}D\overline{\sigma}^d + \frac{1}{2}\overline{\xi}^d K_h^d \overline{\xi}^d \tag{13}$$

The strain-strain relation is deduced as:

$$\overline{\sigma}^d = D^{-1}\overline{\varepsilon}^d \text{ with } D \in [E_c^{-1}, \infty) \tag{14}$$

where E_c is the concrete young modulus. The hardening law takes a linear form $\overline{q}^d = K_h^d \overline{\xi}^d$ where K_h^d is the hardening modulus which is different in compression and traction. The damage criteria are defined by the following damage surface

$$\overline{\phi}^d = |\overline{\sigma}^d| - (\sigma_i^d - \overline{q}^d) \leq 0 \tag{15}$$

$$\sigma_i^d = \begin{cases} \sigma_c^d \text{ for compression} \\ \sigma_t^d \text{ for traction} \end{cases}$$

3.2 Steel

The steel fibers are modeled with an elastoplastic model with isotropic hardening. The classical decomposition of the continuous strain into elastic and plastic terms is assumed:

$$\overline{\varepsilon} = \overline{\varepsilon}^e + \overline{\varepsilon}^p \tag{16}$$

The thermodynamic free energy is expressed in terms of the internal variables: the elastic deformation $\overline{\varepsilon}^e$ and the strain-like hardening variable $\overline{\xi}^s$.

$$\overline{\Psi}^s(\overline{\varepsilon}^e, \overline{\xi}^s) = \frac{1}{2}\overline{\varepsilon}^e E^s \overline{\varepsilon}^e + \frac{1}{2}\overline{\xi}^s K_h^s \overline{\xi}^s \tag{17}$$

where E^s is the steel elastic modulus and K_h^s is the steel hardening modulus. The stress/strain relation reads

$$\overline{\sigma}^s = E^s(\varepsilon - \overline{\varepsilon}^e) \text{ with } \begin{cases} \dot{\overline{\varepsilon}}^p = \dot{\gamma}\dfrac{\partial \overline{\phi}^s}{\partial \sigma} \\ \dot{\overline{\xi}}^s = \dot{\gamma}\dfrac{\partial \overline{\phi}^s}{\partial q} \end{cases} \tag{18}$$

where $\overline{q}^s$ is the stress-like variable defining the linear hardening law $\overline{q}^s = K_h^s \overline{\xi}$ and $\overline{\phi}^s$ is the elastic yield surface:

$$\overline{\phi}^s = |\overline{\sigma}^s| - (\overline{\sigma}_e^s - \overline{q}^s) \leq 0. \tag{19}$$

3.3 Cohesive material behavior at discontinuity

Linear cohesive laws are adopted. The thermodynamic free energies relative to concrete and steel are:

$$\overline{\overline{\Psi}}^d = \tfrac{1}{2}K_{coh}^{d^2}\overline{\overline{\xi}}^d \quad , \quad \overline{\overline{\Psi}}^s = \tfrac{1}{2}K_{coh}^{s^2}\overline{\overline{\xi}}^s \tag{20}$$

where K_{coh} is the softening modulus (< 0) of the cohesive material. The cohesive laws are expressed as a relation between the traction at the discontinuity and the discontinuity variable:

$$t^d = K^d_{coh}\alpha^d \quad , \quad t^s = K^s_{coh}\alpha^s \tag{21}$$

In order to pass from the continuum model to the discrete one, a failure criteria should be verified. This criteria is defined by the function $\overline{\overline{\phi}}$ such that:

$$\overline{\overline{\phi}}^i = |t(\alpha^i)| - (\sigma^i_u - \overline{\overline{q}}^i) \leq 0 \tag{22}$$

where $\overline{\overline{q}}^i = -\frac{\partial \overline{\overline{\Psi}}^i}{\partial \overline{\overline{\xi}}^i} = -K^i_{coh}\overline{\overline{\xi}}^i$ and $i = \{d, s\}$.

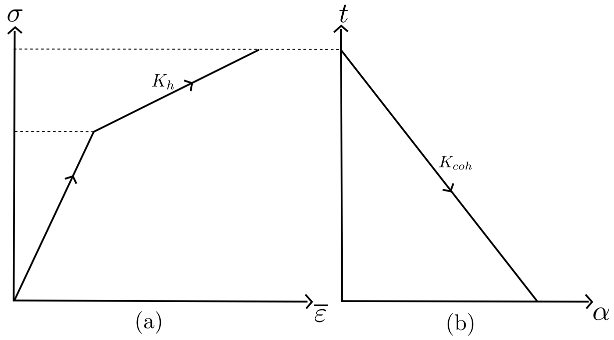

Figure 2: (a) Continuous model ; (b) Discontinuous model

The shear components for both models are supposed linear elastic and therefore the fiber shear stress becomes:

$$\tau = kG\gamma, \tag{23}$$

where k is the shear correction coefficient, G is the shear modulus and γ is the fiber elastic shear strain.

4 Variational formulation

Following the Hu-Washizu variational formulation [29], [30], the variational formulation leads to the following set of nonlinear equations,

$$\bigwedge_{e=1}^{n_{elem}} \bigwedge_{f=1}^{n^{act}_{fib}} \left[f^{int}_{e,f}(U_e, \alpha_{e,f}) - f^{ext}_{e,f}\right] = 0 \tag{24}$$

$$h_{e,f}(U_e, \alpha_{e,f}) = 0, \forall e \in [1, n_{elm}], \forall f \in [1, n^{act}_{fib}] \tag{25}$$

where $\bigwedge$ denotes the assembly operator and n^{act}_{fib} indicates the fibers with active discontinuity. The first equation concerns the global equilibrium while the second is relative to the local equilibrium corresponding to the active embedded discontinuities in the fibers (n^{act}_{fib}).

The linearized form of the system of equations (24) at incremental pseudo-time $n+1$ and iteration $k+1$ reads

$$\bigwedge_{e=1}^{n_{elem}} \bigwedge_{f=1}^{n^{act}_{fib}} \left\{ \begin{bmatrix} K_{BB} & K_{BG} \\ K_{GB} & K_{GG} + K_{coh} \end{bmatrix}^k_{n+1} \begin{bmatrix} \Delta U_{e,f} \\ \Delta \alpha_{e,f} \end{bmatrix}^{k+1}_{n+1} = \begin{bmatrix} f^{int}_{e,f} - f^{ext}_{e,f} \\ h_{e,f} \end{bmatrix}^k_{n+1} \right\} \tag{26}$$

where

$$K_{BB} = \frac{\partial f_{e,f}^{int}}{\partial U_{e,f}} = \int_{V_f} B_f^T K_f B_f dV_f; \tag{27}$$

$$K_{BG} = \frac{\partial f_{e,f}^{int}}{\partial \alpha_{e,f}} = \int_{V_f} B_f^T K_f G_f dV_f; \tag{28}$$

$$K_{GB} = \frac{\partial h_{e,f}}{\partial U_{e,f}} = \int_{V_f} G_f^T K_f B_f dV_f; \tag{29}$$

$$K_{GG} = \frac{\partial h_{e,f}}{\partial \alpha_{e,f}} = \int_{V_f} G_f^T K_f G_f dV_f; \tag{30}$$

with B^f representing the interpolation function of the strain field at the fiber level, G^f the enhanced interpolation function, $U_{e,f}$ the nodal displacements of the fiber and K_f the material tangent modulus of the fiber.

The local equilibrium equation represented by the second equation of the linearized system (26) is solved locally for the active discontinuities, providing the jump increment $\Delta\alpha_{e,f}$. Using the static condensation technique, the condensed fiber stiffness is finally found:

$$K_{cond} = K_{BB} - K_{BG} K_{GG}^{-1} K_{GB} \tag{31}$$

5 Numerical applications

To illustrate the performance of the new Timoshenko multi-fiber beam with embedded discontinuities for seismic problems, two numerical applications are presented hereafter.

5.1 Case study 1 - Eigenmodal analysis

The experimental results of Corn [1] are used hereafter. Consider an homogeneous Timoshenko beam of circular cross-section with a length $L = 257.8$ mm. The material of the beam is Dural (AU4G) with a density of 277 Kg.m^3, a Young modulus of 7.2×10^{10} Pa and a Poisson coefficient equal to 0.3. The boundary conditions are free-free. For more details about the beam instrumentation, the reader is refer to [1]. The purpose of the experiment was to measure the beam eigenfrequencies.

We compare hereafter the experimental results with the eigenfrequencies obtained numerically using the FCQ formulation. To do so, the beam is discretized with 100 FCQ elements. The first six eigenfrequencies and the relative errors between the experimental and the numerical results are presented in the following table:

Mode	Experience	FCQ	
n^o	f_{exp} (Hz)	f_{FE} (Hz)	error (%)
1	4957	4953	0.44
2	10542	10467	0.71
3	16476	16378	0.59
4	20514	20684	0.83
5	24439	25007	2.32
6	24679	25174	2.01

Table 1: Eigenmodal analysis: Experimental versus numerical results

It can be clearly seen that the natural frequencies obtained with the FCQ formulation are very close to the experimental eigenfrequencies and this even for the higher modes.

5.2 Case study 2 - Reinforced concrete column

In order to validate the performance of the multi-fiber displacement based Timoshenko finite element with embedded discontinuities an experimental study made in the Joint Research Center in Italy [31] is used hereafter. During the tests, twelve identical cantilever-type column specimens were subjected to several load paths of cyclic uniaxial or biaxial flexure and to imposed axial loads, to provide data for the development and calibration of numerical models for columns subjected to biaxial bending. Each column had a 25 cm^2 cross section, a free length of 1.5 m and was fixed at the base. Longitudinal reinforcement consisted of eight 16 mm diameter bars, uniformly distributed around the section perimeter (see figure (3)). More details about the experiment can be found in [31].

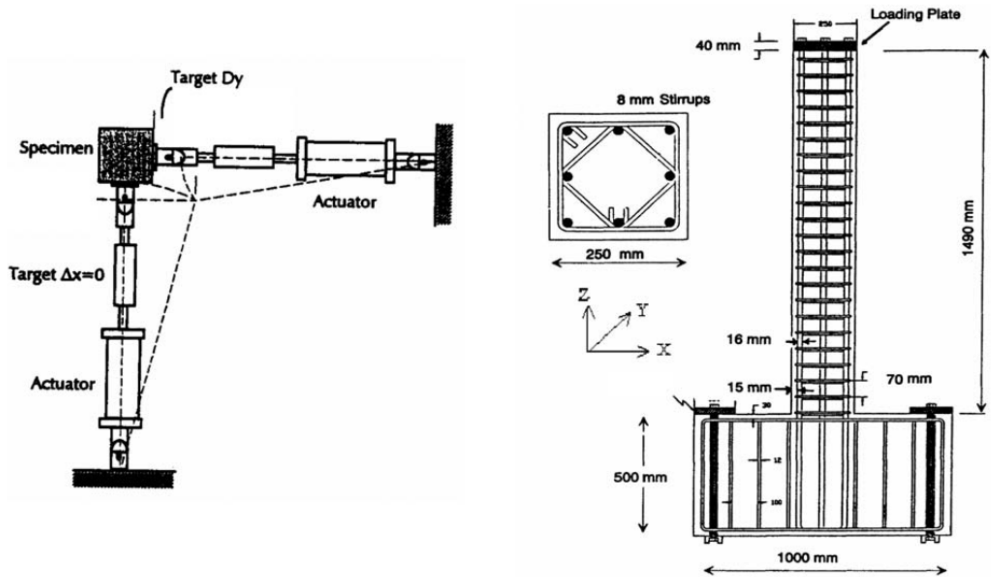

Figure 3: Experimental setup of the reinforced concrete column [31]

In [9], the authors were able to reproduce the experimental cyclic behavior of the $S1$ column using the FCQ multi-fiber Timoshenko beam without any embedded discontinuities. In figure (4), we present the results with the new formulation considering the embedded discontinuities. For this, the column in discretized into 5 FCQ elements, the beam section with 18 fibers and an increasing monotonic loading is applied. One can see that the model reproduces correctly the monotonic envelop curves and captures failure around 8.5×10^4 N.

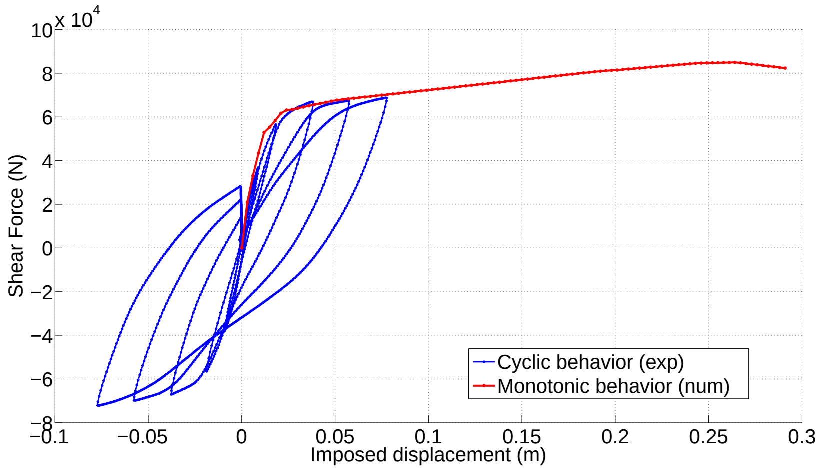

Figure 4: S1 column: experimental versus numerical results

Figures (5),(6) depict the crack openings (discontinuities) in the beam. One can notice that discontinuities appear on the concrete fibers of the first element and decrease along the height of the section. This example shows that the proposed simplified enhanced multi-fiber beam model can simulate the global behavior of the beam providing also access to local information such as crack openings.

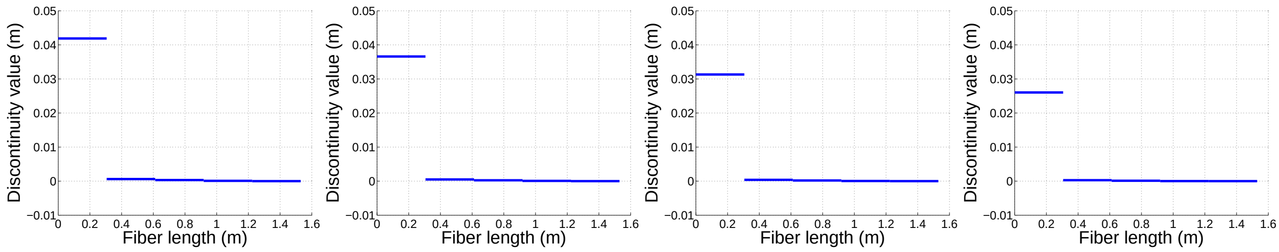

(a) Fiber 1 (b) Fiber 2 (c) Fiber 3 (d) Fiber 4

Figure 5: Discontinuities values in the fiber along the beam

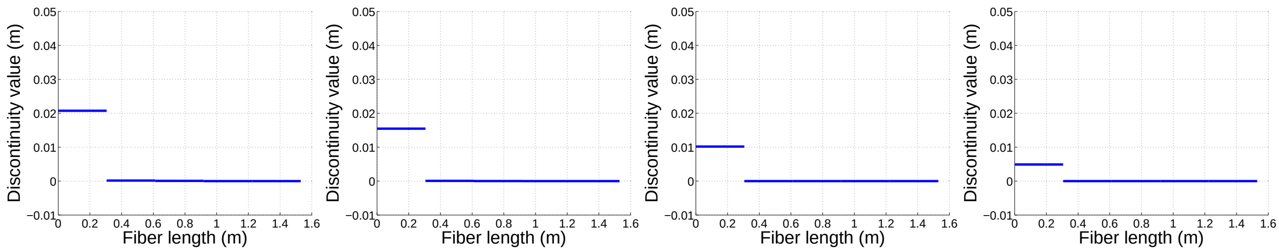

(a) Fiber 5 (b) Fiber 6 (c) Fiber 7 (d) Fiber 8

Figure 6: Discontinuities values in the fibers along the beam

6 Conclusion

In this paper, a new multi-fiber displacement based Timoshenko finite element beam is proposed. Higher order shape functions with additional internal degrees of freedom are used to interpolate the element displacement field and the embedded discontinuity approach is adopted to enhance the fiber kinematic. Each material is modeled with a continuous model to describe the bulk behavior and a cohesive model to illustrate the localized zones. The variational formulation is briefly described. Numerical illustrations are provided in terms of an eigenmodal analysis and the numerical simulation of a reinforced concrete column.

Acknowledgments
The authors would like to thank the PIA-SINAPS@ project (Sésisme et Installation Nucléaire: Améliorer et Pérenniser la Sureté), approved and funded by the National Agency of Research (ANR) following the RSNR 2012 call for projects on future investments post-Fukoshima. (SINAPS@ ANR-11-RSNR-0022)

REFERENCES

[1] S. Corn, Simplification de modèles éléments finis de structures à comportement dynamique de poutre., Ph.D. thesis (1998).

[2] D. R. Owen, E. Hinton, Finite elements in plasticity, Pineridge press, 1980.

[3] P. Kotronis, F. Ragueneau, J. Mazars, A simplified modelling strategy for R/C walls satisfying PS92 and EC8 design, Engineering Structures 27 (8) (2005) 1197–1208.

[4] S. Grange, P. Kotronis, J. Mazars, Numerical modelling of the seismic behaviour of a 7-story building: NEES benchmark, Materials and Structures 42 (10) (2008) 1433–1442.

[5] S. Grange, L. Botrugno, P. Kotronis, C. Tamagnini, The effects of Soil-Structure Interaction on a reinforced concrete viaduct, Earthquake Engineering & Structural Dynamics 41 (11) (2011) 1549–1568.

[6] C. Desprez, P. Kotronis, J. Mazars, Seismic vulnerability assessment of a RC structure before and after FRP retrofitting, Bulletin of Earthquake Engineering 13 (2015) 539–564.

[7] J. Mazars, P. Kotronis, F. Ragueneau, G. Casaux, Using multifiber beams to account for shear and torsion, Computer Methods in Applied Mechanics and Engineering 195 (52) (2006) 7264–7281.

[8] C. Desprez, J. Mazars, P. Kotronis, P. Paultre, Damage model for FRP-confined concrete columns under cyclic loading, Engineering Structures 48 (2013) 519–531.

[9] D. Caillerie, P. Kotronis, R. Cybulski, A Timoshenko finite element straight beam with internam degrees of freedom, International Journal for Numerical and Analytical Methods in Geomechanics 39 (16) (2015) 1753–1773.

[10] I. Bitar, S. Grange, P. Kotronis, N. Benkemoun, A review on Timoshenko multi-fiber beams Finite Element formulations and elasto-plastic applications (under review), European Journal of Environnemental and Civil Engineering.

[11] P. Pegon, A Timoshenko simple beam element in Castem 2000.

[12] J. Guedes, P. Pegon, A. V. Pinto, A Fibre/Timoshenko beam element in Castem 2000.

[13] F. Armero, Large-scale modeling of localized dissipative mechanisms in a local continuum: Applications to the numerical simulation of strain localization in rate-dependent inelastic solids, Mechanics of Cohesive-Frictional Materials 4 (March 1998) (1999) 101–131.

[14] A. Needleman, Material rate dependence and mesh sensitivity in localization problems, Computer Methods in Applied Mechanics and Engineering 67 (1) (1988) 69–85.

[15] A. Hillerborg, Application of fracture mechanics to concrete: summary of a series of lectures 1988, Div of Building Materials LTH, Lund university, 1988.

[16] Z. P. Bažant, T. B. Belytschko, Wave propagation in a strain-softening bar: exact solution, Journal of Engineering Mechanics 111 (3) (1985) 381–389.

[17] Z. P. Bažant, J. Pan, G. Pijaudier?Cabot, Softening in Reinforced Concrete Beams and Frames, Journal of Structural Engineering 113 (12) (1987) 2333–2347.

[18] R. Chambon, D. Caillerie, N. El Hassan, Etude de la localisation unidimensionnelle à l'aide d'un modèle de second gradient, Comptes rendus de l'Académie des sciences. Série II, Mécanique, physique, chimie, astronomie 323 (4) (1996) 231–238.

[19] M. Ortiz, Y. Leroy, A. Needleman, A finite element method for localized failure analysis, Computer Methods in Applied Mechanics and Engineering 61 (2) (1987) 189–214.

[20] J. C. Simo, J. Oliver, F. Armero, An analysis of strong discontinuities induced by strain-softening in rate-independent inelastic solids, Computational Mechanics 12 (5) (1993) 277–296.

[21] G. Wells, L. Sluys, Application of embedded discontinuities for softening solids, Engineering Fracture Mechanics 65 (2-3) (2000) 263–281.

[22] H. R. Loffi, P. B. Shing ', Embedded Representation of Fracture in Concrete With Mixed Finite Elements, International Journal for Numerical Methods in Engineering 38 (July 1994) (1995) 1307–1325.

[23] M. Jukić, B. Brank, A. Ibrahimbegović, Failure analysis of reinforced concrete frames by beam finite element that combines damage, plasticity and embedded discontinuity, Engineering Structures 75 (2014) 507–527.

[24] F. Armero, On the characterization of localized solutions in inelastic solids: an analysis of wave propagation in a softening bar, Computer Methods in Applied Mechanics and Engineering 191 (3-5) (2001) 181–213.

[25] D. Ehrlich, F. Armero, Finite element methods for the analysis of softening plastic hinges in beams and frames, Computational Mechanics 35 (4) (2005) 237–264.

[26] B. H. Pham, D. Brancherie, L. Davenne, A. Ibrahimbegović, Stress-resultant models for ultimate load design of reinforced concrete frames and multi-scale parameter estimates, Computational Mechanics 51 (3) (2013) 347–360.

[27] A. Ibrahimbegović, D. Brancherie, Combined hardening and softening constitutive model of plasticity: Precursor to shear slip line failure, Computational Mechanics 31 (1-2 SPEC.) (2003) 88–100.

[28] M. Ortiz, A constitutive theory for the inelastic behavior of concrete 4 (1985) 67–93.

[29] K. Washizu, Variational methods in elasticity and plasticity, Vol. 9, 1984.

[30] T. B. Belytschko, J. Fish, B. E. Engelmann, A finite element with embedded localization zones* 70 (1988) 59–89.

[31] S. N. Bousias, G. Verzeletti, M. N. Fardis, E. Gutierrez, Load-Path Effects in Column Biaxial Bending with Axial Force, Journal of Engineering Mechanics 121 (5) (1995) 596–605.